Numerical procedure for analyzing impurity-induced resonant-state STM images observed in high-T_c superconductors

Qian Wang[1] and Chia-Ren Hu[2]
[1]*Texas Center for Superconductivity, University of Houston, Houston, Texas 77204, USA*
[2]*Department of Physics, Texas A&M University, College Station, Texas 77843, USA*
(Received 22 September 2003; revised manuscript received 17 February 2004; published 27 September 2004)

Numerical procedure is developed for analyzing impurity-induced resonant-state STM images observed in high-T_c superconductors, and is applied to three sets of higher resolution data provided to us by J. C. Seamus Davis and E. W. Hudson. Each image is associated with a Zn impurity in $Bi_2Sr_2CaCu_2O_8$. The averaged, integrated, relative quasiparticle local density of states at all predominant Cu(Zn)-sites near a Zn impurity is extracted. The results can be used to test the predictions of all existing and future tight-binding-type theories on such images.

DOI: 10.1103/PhysRevB.70.092505 PACS number(s): 74.50.+r, 68.37.Ef, 74.72.−h, 74.20.Rp

Scanning a low-temperature scanning tunneling microscope (STM) on a cleaved $Bi_2Sr_2CaCu_2O_8$ (BSCCO) single crystal at a fixed bias energy, Pan *et al.* observed images localized near individual Zn impurities in the topmost CuO_2 plane,[1] when the bias voltage is set at the peak of a near-zero-energy resonance. Figure 1 shows a typical such image.

Understanding this resonant-state image (RSI) is a great challenge. Due to the past several years of studies, it has been widely accepted that high-T_c superconductors have a $d_{x^2-y^2}$-wave pairing symmetry. The difference between this symmetry and the conventional *s*-wave symmetry is: A gap function (or pair potential) with this symmetry has line nodes parallel to the *c*-axis along the $\{11\}$, $\{1\bar{1}\}$, $\{\bar{1}1\}$, and $\{\bar{1}\bar{1}\}$ directions in the *ab* plane on a nearly cylindrical Fermi surface, and changes sign across any of these nodal lines, whereas *s*-wave symmetry would imply no sign change. Many theorists have shown that a unitary impurity in a *d*-wave superconductor can lead to two essentially degenerate resonant states per spin of almost zero energy which are quasi-bound to the impurity. (These near-zero-energy resonances are close kins of the midgap states predicted by one of us.[2]) The predicted spectral peak-feature near zero bias[3] agrees with observations very well,[4] but the predicted RSIs based solely on the wave functions of these resonant states differ dramatically from the observed ones. For example, Figs. 6(a) and 6(b) of Ref. 5 have given such an image. They show a vanishing quasiparticle local density of states (LDOS) at the unitary impurity site and largest LDOS at the four nearest-neighbor sites, which differ sharply with the observation shown in Fig. 1, where the largest LDOS is at the center (impurity) site, and nearly vanishing LDOS at the four nearest-neighbor sites. *This disagrement is a model-independent conclusion,* since a RS wave function must vanish at the site of a unitary impurity, and a nonunitary imputity can not give a near zero-energy resonance. The disagreement also extends to the second and third nearest neighbor sites, where both the measured and calculated LDOS are not small. Two tight-binding-type theories have been offerred to explain this disagreement.[5,6] Namely, finite LDOS are predicted at the Zn or Cu sites only, with no continuous LDOS between these lattice sites. This is of course not what has been observed, which is quasi-continuous, as is shown in Fig. 1. Thus to compare experimental data with these theories, it is necessary to convert the measured data to a set of discrete LDOS at the Cu or Zn sites, by performing some integration.

Each set of experimental data provided to us has two STM images. One is a topographic image (an energy-integrated spatial image), which gives the top BiO layer, showing only the Bi atoms. They are observed to be displaced from their ideal orthorhombic lattice sites, forming a supermodulation with a wave vector along the *b*-axis. According to the crystal structure of BSCCO, Bi atoms are above the Cu atoms, or the Zn impurity atoms substituting for Cu. The other image, such as shown in Fig. 1, is taken with STM in the same local area, but with the bias voltage set essentially at the peak of a near-zero-energy resonance. The higher resolution date taken are made of 128×128 intensities points. Each bright spot in the Fig. 1 spreads about 5 points in each direction. The spread of each spot is due to at least two effects — electron wave function and thermo-smearing. These bright spots are seen to spread into and

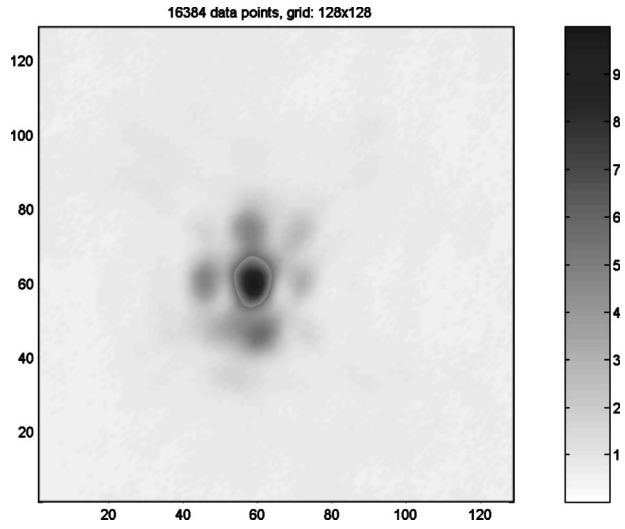

FIG. 1. A typical resonant-state STM image observed by Pan *et al.* near a Zn impurity in BSCCO, when the bias voltage is set at the peak of a near-zero-energy resonance. The *a* and *b* crystal axes are essentially along the diagonals.

overlaps with each other. That is, contribution from one Cu(Zn) site tails into neighboring sites. Thus to simply integrate the intensity over a unit-cell region around each lattice site can not give a correct estimate. We have thus developed a generally useful numerical tool for estimating the integrated intensity associated with each lattice site around an impurity.

The intensity contributed by a single Cu(Zn) site is assumed to be a generalized Gaussian based on three reasons: (1) The exact form of the contributing electronic wave function is unknown. The electron wave function at a Cu site is $d_{x^2-y^2}$, but tunneling might be via some higher s-orbitals. Besides, this $d_{x^2-y^2}$ orbital should still hybridize with the nearest oxygen p_x or P_y orbitals.[7] Two atomic layers exist above the topmost CuO_2 plane: A BiO layer at the top is believed to be semiconducting. Below it is a SrO layer, which is believed to be insulating. Ions residing on these two layers may interfere with the measurement of any state in the CuO_2 plane.[5,6] (2) Thermo-smearing effect and experimental limitations in resolution should be modeled by Gaussians. (3) The generalized Gaussian function is the simplest form we can use which can take into account many features of the peaks in the observed data, such as position, intensity, width, anisotropy, orientation, etc. In addition, the more accurate data that are provided to us for analysis are taken on 128×128 points, and each bright spot covers about 5-points by 5 points. If we use a more complicated function to model the contribution from each lattice site, the number of parameters needed may be too large. Then we may not be able to determine all parameter values accurately from the given data.

Thus the intensity peak at each site i is assumed to take the form $I(x,y)=\exp(a_{1i}+a_{2i}x+a_{3i}y+a_{4i}x^2+a_{5i}xy+a_{6i}y^2)$, where a_{ji}, $j=1$ to 6, are parameters to be estimated. The total number of parameters is 6 times the number of peaks, n, which is an input by the user, and should be larger than the number of predominant peaks. After obtaining the parameters, the integrated intensity at site i can be obtained:

$$I_i = 2\pi \frac{\exp\left(a_{1i} - \dfrac{a_{5i}a_{2i}^2 + a_{4i}a_{4i}^2 - a_{6i}a_{2i}a_{3i}}{4a_{4i}a_{5i} - a_{6i}^2}\right)}{\sqrt{4a_{4i}a_{5i} - a_{6i}^2}}, \qquad (1)$$

for $a_{3i}<0$, $a_{4i}<0$, and $a_{5i}^2-4a_{3i}a_{4i}<0$. Otherwise the integrated intensity at this site will be set as zero. (These inequalities ensure that the generalized Gaussian is not pathological.)

An iterative procedure is used to estimate the parameters:

(1) Initialize all the parameters so that each peak intensity is very small, by setting each a_{1i} negative and large.

(2) Let $i=1$, which refers to the highest peak in the data.

(3) From the data, subtract out all contributions from all Gaussian peaks other than i. This step initially does little change to the data, but in later iterations, it will substract out all Gaussian peaks already found.

(4) Gaussian fit the remaining data around the highest point, and obtain 6 parameters for the peak i. The fitting region is taken to be somewhat smaller than a unit cell, since the weak-intensity region is more likely influenced by the neighboring contributions. When conditions $a_{3i}<0$, $a_{4i}<0$, and $a_{5i}^2-4a_{3i}a_{4i}<0$ are not met, we set a_{1i} negative and large, so site i is not considered a peak and will not be substracted in the following iterations.

(5) Let $i=i+1$, which refers to the next highest peak (obtained with a computer search), and go back to step 3.

(1) Continue this procedure as long as $i\leqslant n$.

(7) Repeat 2 through 6 several times in order to improve the separation of the individual peak contributions. Stop iteration when the so-obtained parameter values stop changing within a given accuracy. Usually three to four iterations are sufficient.

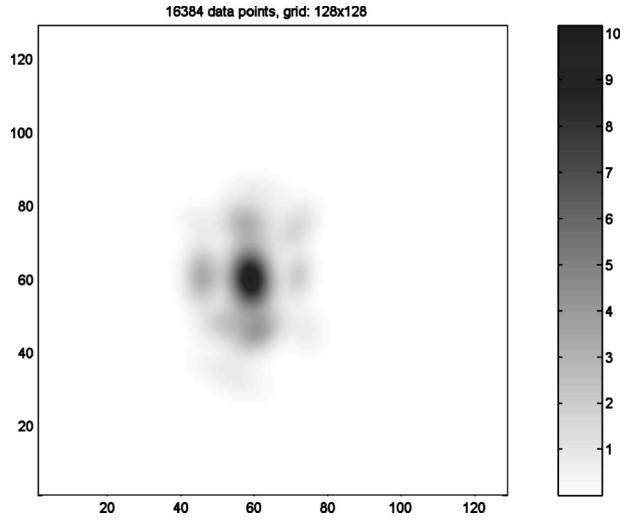

FIG. 2. Density plot of a fitted image obtained from the observed image in Fig. 1. We have put $n=15$, so it can only reproduce the 15 most prominant peaks in the actual image.

Three higher-resolution RSIs are analyzed, each taken on 128×128 points around a Zn site. We have set $n=15$, which is larger than the number of predominant peaks, which is about 9. The total number of fitting parameters is then 90. We believe that without the scheme devised here, it would be impossible to determine so many fitting parameters accurately. If higher resolution data could become available in the future, we think that this input number can still be increased to include the weaker peaks, thereby allowing more stringent tests of theories.

Figure 2 shows the density plot of the image obtained by fitting the actual STM image shown in Fig. 1. It is seen that the fitted image gives all predominant peaks and looks very similar to the actual image. For a more detailed comparison we have plotted, in Figs. 3, these two images along a vertical line and a horizontal line [the (11) and $(1\bar{1})$ crystal directions] that pass through the central peak. Similar plots along two diagoanal lines [the (01) and (10) crystal directions] are given in Fig. 4. The fitting is very good, although there are still some discrepancies. The position, width and height of each fitted peak are seen to be very close to those of the actual data.

We have applied our method on three sets of 128×128 data provided to us, and have obtained from them the averaged, integrated, relative intensities of LDOS, which are normalized to unity at the central Zn-impurity site. (Many

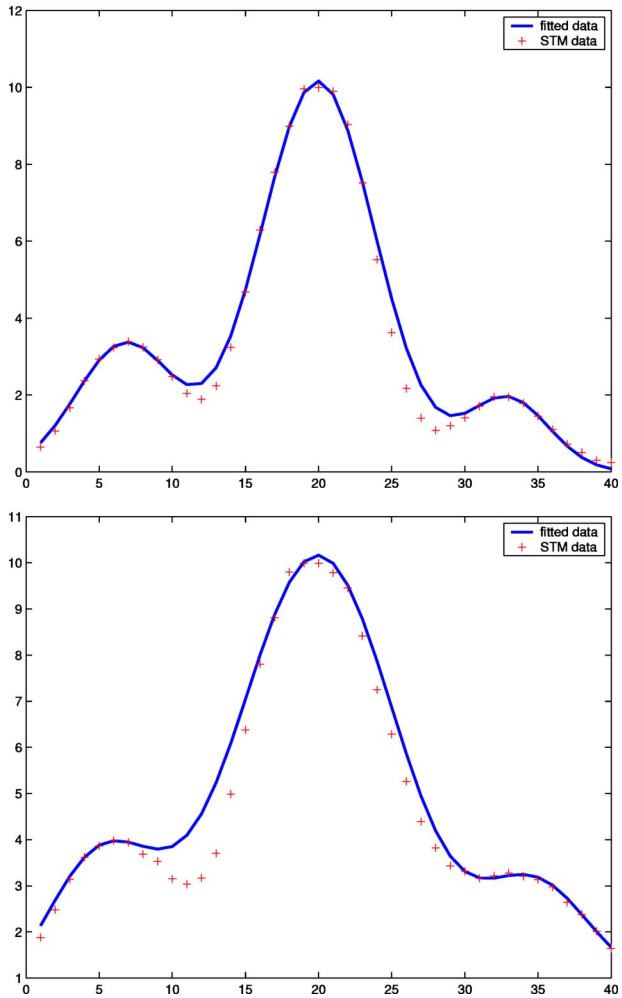

FIG. 3. (Color online) Fitted data (solid lines) and the actual STM data (the + symbols) along a vertical (upper) and a horizontal (lower) line [i.e., the (11) and $(1\bar{1})$ crystal directions] passing through the central peak.

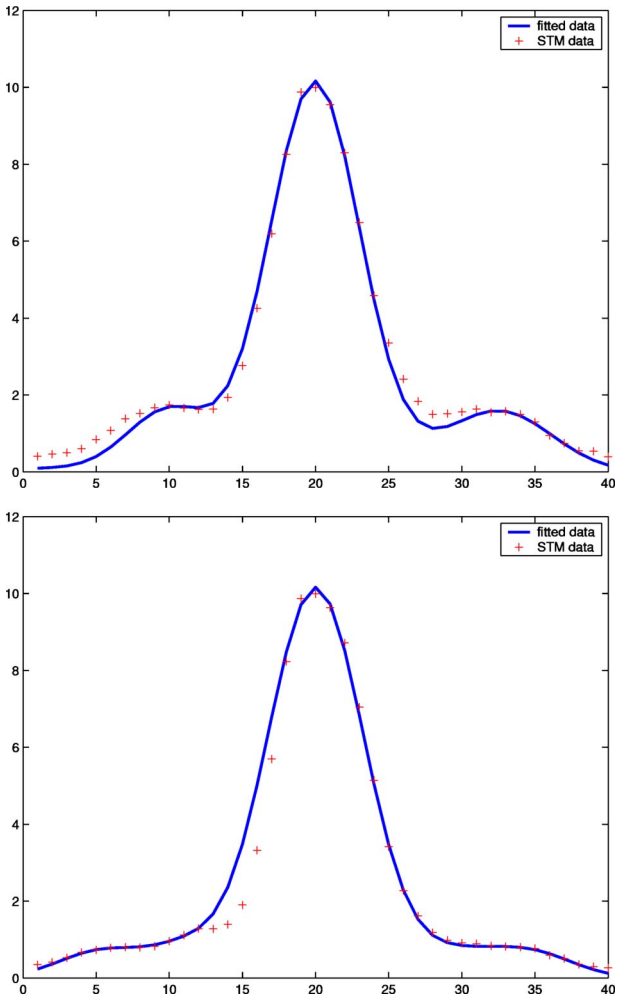

FIG. 4. (Color online) Similar to the previous figure, except that the fitted data and and actual STM data are along two diagonal lines [i.e., in the (10) and (01) crystal directions], which pass through the central peak.

64×64 data sets provided to us do not have the resolution for this analysis. There are also two 128×128 data sets which correspond to a different type of RSI. We have not included them in our averaging process, because we suspect that they may correspond to a Zn impurity in a different local environment.) The average is done over the three useable images and also over all equivalent sites in each image to restore square symmetry — For example, average over the (01), (10), $(0\bar{1})$, and $(\bar{1}0)$ sites is reported as the result at all these sites. It is to remove features unique to any single image and also features so far not taken into account in theories. The results are shown in Fig. 5, with the relative intensities of LDOS presented by the areas of the circles. These averaged, integrated, relative intensities of LDOS are 1.00 at the (00) site, 0.02 at the (01)-equivalent sites, 0.32 at the (11)-equivalent sites, and 0.13 at the (02)-equivalent sites. These values can be used to test the validity of any existing or future tight-binding-type theories of such images, which do not take into account any superlattice-like distortions of the lattice. (After removing the orientation averaging, our results can also be used to test theories which do take into account such distortions.) For example, Ref. 5 has provided a theory which is based on a blocking model. In that work, a very crude comparison of the predicted values of that theory with the measured values at the lattice sites has been made. But as has been explained there, the measured intensity of LDOS is a quasi-continuous function of position, rather than existing at the lattice sites only, so some integration should be performed on the measured data before they could be

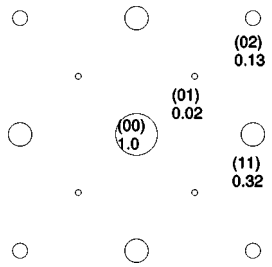

FIG. 5. Integrated relative intensity of LDOS normalized to unity at the central peak extracted from our analysis. These results have been averaged over three sets of data and also over all equivalent sites to restore perfect square symmetry.

TABLE I. Comparison between the measured LDOS at the near-zero-bias resonant energy by Pan *et al.* (Ref. 1), and the blocking-model predictions of Ref. 5, at the nearest neighbor sites (10) and (01), the next nearest neighbor site (11), and the third nearest neighbor sites (20) and (02), after normalizing both sets of data to unity at the Zn impurity site (00). Row one: the measured LDOS at the lattice sites around the Zn impurity, used in Ref. 5 for crude comparison. Row two: An integrated set of intensities of LDOS obtained in the present analysis. Row three: The prediction of such intensities from Ref. 5 based on a blocking model introduced there.

(00)	(10) & (01)	(11)	(20) & (02)
1.00	0.18	0.29	0.13
1.00	0.02	0.32	0.13
1.000	0.068	0.593	0.384

compared with the predictions of any tight-binding type of theories. This is the main reason that this work is done, so in Table I we have made a new comparison. Row one of this table gives the measured data used in Ref. 5 which is really incorrect because it didn't employ any spatial integration, but is simply the measured intensity of LDOS at the lattice sites. It was used there for a very crude comparison between theory and experiment only. Row three gives the predicted values of Ref. 5 based on a blocking model introduced there. The discrepancy between row one and row three cannot be taken seriously for the reason already given in Ref. 5, which has been repeated above. Row two of this table gives a set of integrated intensities of LDOS obtained in this analysis. We see that the main difference between rows one and two is in the values at the (01)-equivalent sites. Clearly this is because the tall central peak has tailed substantially into the (10) and (01) sites. This fact further supports the conclusion that row one should not be used for comparison with row three, revealing the necessity of this analysis. The discrepancy between row two and row three is much more likely to be a genuine discrepancy, and likely indicates that the model needs to be improved. Reference 6 did not provide such numbers for a similar comparison, but it should be done to test its validity.

In conclusion, a generally useful tool is developed for analyzing impurity-induced resonant-state images observed in high-T_c superconductors. The purpose is to convert the actually observed quasi-continuous image to a discrete set of integrated intensities, one for a lattice site of a square lattice, so it can be compared with the predictions of tight-binding-type theories of such images which treat a CuO_2 plane as a simple square lattice for holes to hop around. This tool should also be useful for analyzing similar such images which might be observed in other systems, for a similar purpose. We assume that the RSI observed by Pan *et al.* near a Zn impurity in BSCCO is made of a sum of n overlapping generalized Gaussian functions, one roughly located at a different lattice site of a two-dimensional (2D) square lattice (but allowing possible shifts from the ideal lattice-site positions). An iteration procedure is introduced which allows the $6n$ parameters in the n generalized Gaussian functions to be determined. (We took $n=15$, which is not the upper limit.) The fitted image agrees very well with the experimentally observed image on all prominant peaks. Normalized LDOS on all predominant sites can then be extracted by integrating each Gaussian functuion. They can be compared with predictions of any tight-binding-type theories which consider a CuO_2 plane as a simple square lattice. If higher resoluction images could be obtained, we could replace the generalized Gaussian function used here with a more complicated model function to do such an analysis, such as some atomic orbital(s), possibly hybridized, convoluted with thermal smearing. Thus this analysis has the potential of finding the correct single-site contribution, thereby revealing useful detailed information about the system. That we found here that generalized Gaussian functions can give excellent fits calls for theorectical understanding, but perhaps higher-resolution data will reveal their inadequacy. Another potential usefulness of this tool is to uncover different local environments for the impurity atoms, such as a Zn impurity paired with an O or Bi vacancy straight above it, an O or Sr vacancy to the side of those sites, or a missing O atom to the side of the Zn atom in the same CuO_2 plane, or a pair of or more Zn impurities in proximity, etc. Discovering these combinations might provide additional information about the system and the underlying mechanism for high temperature superconductivity, and allow more stringent tests of theories on such images.

This work is supported by the Texas Center for Superconductivity and Advanced Materials at the University of Houston. The authors would like to thank J. C. Seamus Davis and Eric W. Hudson for providing the data used in this analysis.

[1] S. H. Pan *et al.*, Nature (London) **403**, 746 (2000).
[2] C.-R. Hu, Phys. Rev. Lett. **72**, 1526 (1994).
[3] See, for example, G. Preosti *et al.*, Phys. Rev. B **50**, 1259 (1994); R. Fehrenbacher *et al.*, *ibid.* **50**, 3495 (1994); A. V. Balatsky *et al.*, *ibid.* **51**, 15 547 (1995); T. Xiang *et al.*, *ibid.* **51**, 11 721 (1995); M. I. Salkola *et al.*, Phys. Rev. Lett. **77**, 1841 (1996); Y. Onishi *et al.*, J. Phys. Soc. Jpn. **65**, 675 (1996); M. E. Flatte *et al.*, Phys. Rev. Lett. **80**, 4546 (1998); K. Kuboki *et al.*, Physica B **259-261**, 460 (1999); M. E. Flatte, Phys. Rev. B **61**, R14 920 (2000); H. Tsuchiura *et al.*, J. Phys. Chem. Solids **84**, 3165 (2000); H. Tsuchiura *et al.*, Phys. Rev. Lett. **62**, 265 (2001), etc. Later references are too numerous to all cite here.
[4] A. Yazdani *et al.*, Phys. Rev. Lett. **83**, 176 (1999); E. W. Hudson *et al.*, Science **285**, 88 (1999); and Ref. 1.
[5] J.-X. Zhu *et al.*, Phys. Rev. B **62**, 6027 (2000).
[6] I. Martin *et al.*, Phys. Rev. Lett. **88**, 097003 (2002).
[7] F. C. Zhang *et al.*, Phys. Rev. B **37**, 3759 (1988).